ICARUS 77, 148–170 (1989)

Pluto's Atmosphere

J. L. ELLIOT,*† E. W. DUNHAM,* A. S. BOSH,* S. M. SLIVAN,*
L. A. YOUNG,* L. H. WASSERMAN,‡ AND R. L. MILLIS‡

Department of Earth, Atmospheric, and Planetary Sciences, and †Department of Physics, Massachusetts Institute of Technology, Cambridge, Massachusetts 02139; and ‡Lowell Observatory, Flagstaff, Arizona 86001

Received August 27, 1988; revised October 12, 1988

The stellar occultation by Pluto on June 9, 1988, was observed with a high-speed CCD photometer attached to the 0.9-m telescope aboard NASA's Kuiper Airborne Observatory (KAO). The occultation lightcurve, which probed two regions on the sunrise limb separated by about 2000 km, reveals a clear upper atmosphere that overlies an extinction layer with an abrupt upper boundary. The observations demonstrate that the extinction layer extends along the portion of the sunrise limb bounded by the immersion and emersion regions, as well as along the corresponding portion of the sunset limb on the opposite side of the planet. In all, the total limb probed by the KAO data for extinction represents nearly half of Pluto's circumference. Hence, the extinction layer may surround the entire planet. A model atmosphere is presented, from which is derived an occultation lightcurve that closely matches the data. In addition to the standard parameters describing the occultation curve by an isothermal atmosphere, our model includes the radius of the upper boundary of the extinction and the radius of unit observed optical depth as free parameters. Fits of this model to the immersion and emersion lightcurves show no significant differences in the derived atmospheric structure. A preliminary geometrical solution, based on three occultation chords, yields a half-light radius of 1214 ± 20 km. At this level, the mean scale height derived from the model fits to the KAO data is 59.7 ± 1.5 km. The corresponding ratio of temperature to mean molecular weight is 4.2 ± 0.4°K/amu, with the principal source of error arising from the uncertainty in the mass of Pluto. The extinction layer, whose upper boundary lies 25 km below the half-light level, has a minimum thickness of 46 km, a minimum vertical optical depth of 0.19, and a scale height of 33.4 ± 6.9 km. For a pure methane atmosphere, our results imply (for the clear atmosphere at the half-light level) a temperature of 67 ± 6°K, a number density of 8.3×10^{13} cm^{-3}, and a pressure of 0.78 μbar. Our occultation data are also consistent with a predominantly nitrogen atmosphere (such as that of Titan), in which case the temperature would be 117 ± 11°K. The substantially smaller scale height of the extinction layer may arise from properties of the "particles" causing the extinction or may indicate a lower temperature in this region. Since our analysis indicates that the extinction layer is optically thick at the limb of Pluto, determinations of Pluto's radius by methods that use reflected light, such as speckle interferometry and observations of the mutual events, give results that refer to the *visible disk* of Pluto and not to the planet's solid surface. Unit optical depth of the extinction layer (observed along the line of sight) lies at 1174 ± 20 km, a level consistent with the radius of Pluto derived from the mutual events (1142 ± 21 km). The mutual event radius is also consistent with the deepest level probed by the occultation: it lies at a radius of 1143 ± 20 km, which represents an upper limit on the surface radius. For a pure methane atmosphere, a surface pressure as low as 3 μbar (the vapor pressure of methane at 50°K) would be consistent with the occultation data.

0019-1035/89 $3.00

I. INTRODUCTION

Apart from its intrinsic interest, the properties of any Plutonian atmosphere affect several issues that are fundamental to our understanding of the present state and evolution of the planet. An atmosphere has a major effect on regulating the input and subsequent reradiation of solar energy. It provides a buffer between the planetary surface and the space environment, thereby limiting the rate at which surface ice can be lost by sublimation over long time scales. The composition of an atmosphere is intimately related to the composition and physical state of the surface. Hence, knowledge of Pluto's atmospheric composition constrains the possibilities for its bulk composition. Finally, Pluto's atmospheric structure provides information that is essential for the correct interpretation of other observations of Pluto, such as visible and near-infrared spectra, thermal fluxes, and the lightcurves of the mutual occultations and eclipses that are currently being observed for Pluto and its satellite Charon (Binzel *et al.* 1985).

The existence of a detectable atmosphere around Pluto has been uncertain (Cruikshank 1987). Spectra of Pluto show methane bands, which were first interpreted by Cruikshank *et al.* (1976) as evidence for solid methane on the surface of Pluto. Later, Fink *et al.* (1980) obtained spectra with improved signal-to-noise ratio in the near infrared, which, on the basis of saturation of the strong bands, they interpreted as evidence for an atmosphere. More recently, however, Buie and Fink (1987) have observed that the strengths of the methane bands vary with the rotational phase of Pluto. They interpret these variations as evidence that at least some of the methane absorption must be due to frost on Pluto's surface. The presence of solid methane implies that some methane gas will be present, due to the vapor pressure from the solid, but determining the contribution of each to Pluto's spectrum has proven difficult. Infrared fluxes from the Pluto–Charon system measured by IRAS at 25, 60, and 100 μm have been used to set limits on an atmosphere by Tedesco *et al.* (1987), Sykes *et al.* (1987), and Aumann and Walker (1987).

The most sensitive Earth-based method for directly probing the density structure of an atmosphere is based on photometric observations of stellar occultations. Because of Pluto's small angular size and low angular velocity, useful occultations are rare for this planet. In 1965 Pluto was observed to pass nearly in line with a star, but did not occult it. This observation, along with concurrent astrometric measurements of Pluto's path relative to the star, was used to place an upper limit on Pluto's radius (Halliday *et al.* 1966). An attempt to observe a stellar occultation by Pluto in 1980 resulted in a single chord observation of an occultation by its satellite Charon. It showed no detectable atmosphere on Charon, and was used to set a lower limit of 600 km on Charon's radius (Walker 1980). Finally, an observation of an occultation by Pluto in 1985 made under less than ideal conditions has been claimed by Brosch and Mendelson (1985), but these data have not been published.

The June 9, 1988, occultation by Pluto was identified several years ago by Mink and Klemola (1985). Subsequent photometry by Bosh *et al.* (1986) showed the star to be substantially brighter than originally reported. Consequently, a good signal-to-noise ratio could be expected for the observations, even with small telescopes (Millis and Elliot 1979). Refined predictions based on 55 plates taken with the 61-in. Astrometric Reflector at the U.S. Naval Observatory's Flagstaff Station predicted a ground track crossing the South Pacific, New Zealand, and Australia (Wasserman *et al.* 1988). The center of this nearly east–west track passed near latitude −22° and east longitude −170°. Charon, at the time of the occultation, was near southern elongation. Its presence significantly complicated the prediction effort, due to its unknown effect

$$\frac{d\theta}{dr} = \frac{\nu_{STP} n_h \sqrt{2\pi r_h}}{N_0 H_h^{3/2}} u^{-5/2} \left[1 + \frac{1}{8}(\delta u) - \frac{21}{8}(\delta u)^2 + \frac{135}{32}(\delta u)^3\right] \exp\left[\frac{1}{\delta}\left(\frac{1}{u} - 1\right)\right] \quad \text{(A14)}$$

$$\frac{d^2\theta}{dr^2} = \frac{\nu_{STP} n_h \sqrt{2\pi r_h}}{N_0 H_h^{5/2}} u^{-9/2} \left[1 + \frac{21}{8}(\delta u) - \frac{39}{16}(\delta u)^2 + \frac{93}{32}(\delta u)^3 - \frac{135}{64}(\delta u)^4\right] \exp\left[\frac{1}{\delta}\left(\frac{1}{u} - 1\right)\right]. \quad \text{(A15)}$$

Our next task is to establish the value for n_h. We do this by using the condition for half-light, which requires (by definition) that $\phi_{ref} = \frac{1}{2}$ when $r = r_h$ ($u = 1$). Substituting values from Eqs. (A5) and (A6) into Eq. (A3) and setting the result equal to $\frac{1}{2}$, we find

$$\left(1 + D\frac{\theta}{r}\right)\left(1 + D\frac{d\theta}{dr}\right) = 2. \quad \text{(A16)}$$

Solving this equation for n_h, we get the following series solution:

$$n_h = \frac{N_0 H_h^{3/2}}{\nu_{STP} D \sqrt{2\pi r_h}}\left(1 + \frac{15}{8}\delta + \frac{473}{64}\delta^2 + \ldots\right). \quad \text{(A17)}$$

We substitute the above value for n_h into Eqs. (A5)–(A7) and evaluate the terms to second order in δ when $u = 1$:

$$\left.\frac{\rho}{r}\right|_{r=r_h} = 1 - \delta - \frac{3}{2}\delta^2 + \ldots \quad \text{(A18)}$$

$$\left.\frac{d\rho}{dr}\right|_{r=r_h} = 2\left(1 + \delta + \frac{5}{2}\delta^2 + \ldots\right) \quad \text{(A19)}$$

$$\left.\frac{d^2\rho}{dr^2}\right|_{r=r_h} = -\frac{1}{H_h}\left(1 + \frac{9}{2}\delta + \frac{79}{8}\delta^2 + \ldots\right). \quad \text{(A20)}$$

We now take the power series in Eqs. (A18)–(A20) and insert them into Eq. (A4) to achieve the desired value of the light-curve slope at half-light:

$$\left.\frac{d\phi_{ref}}{d\rho}\right|_{r=r_h} = \frac{1}{8H_h}\left(1 + \frac{1}{2}\delta - \frac{57}{8}\delta^2 + \ldots\right). \quad \text{(A21)}$$

Defining the "observed scale height," H_{obs}, as the scale height of a planetary atmosphere that would produce the same slope of the occultation lightcurve in the limit $\delta \to 0$, we can write

$$\left.\frac{d\phi_{ref}}{d\rho}\right|_{r=r_h} = \frac{1}{8H_{obs}}. \quad \text{(A22)}$$

Combining Eqs. (A21) and (A22) we have the following relation between the two scale heights:

$$H_h = H_{obs}\left(1 + \frac{1}{2}\delta - \frac{57}{8}\delta^2 + \ldots\right). \quad \text{(A23)}$$

In order to express H_h entirely in terms of observed quantities, we define $\delta_{obs} = H_{obs}/r_h$. The following equations relate δ and δ_{obs}:

$$\delta_{obs} = \delta\left(1 - \frac{1}{2}\delta + \frac{59}{8}\delta^2 + \ldots\right) \quad \text{(A24)}$$

$$\delta = \delta_{obs}\left(1 + \frac{1}{2}\delta_{obs} - \frac{55}{8}\delta_{obs}^2 + \ldots\right). \quad \text{(A25)}$$

Substituting the series of Eq. (A25) into Eq. (A24) we obtain the desired relation:

$$H_h = H_{obs}\left(1 + \frac{1}{2}\delta_{obs} - \frac{55}{8}\delta_{obs}^2 + \ldots\right). \quad \text{(A26)}$$

We shall also require expressions for the number density and pressure of the atmosphere at the half-light radius (r_h) in terms of the observed scale height:

$$n_h = \frac{N_0 H_{obs}^{3/2}}{\nu_{STP} D \sqrt{2\pi r_h}}\left(1 + \frac{21}{8}\delta - \frac{115}{64}\delta^2 + \ldots\right) = \frac{N_0 H_{obs}^{3/2}}{\nu_{STP} D \sqrt{2\pi r_h}}\left(1 + \frac{21}{8}\delta_{obs} - \frac{31}{64}\delta_{obs}^2 + \ldots\right) \quad \text{(A27)}$$

$$p_h = \frac{\bar{\mu} M_0 g_h N_0 H_{obs}^{5/2}}{\nu_{STP} D \sqrt{2\pi r_h}}\left(1 + \frac{25}{8}\delta - \frac{487}{64}\delta^2 + \ldots\right) = \frac{\bar{\mu} M_0 g_h N_0 H_{obs}^{5/2}}{\nu_{STP} D \sqrt{2\pi r_h}}\left(1 + \frac{25}{8}\delta_{obs} - \frac{387}{64}\delta_{obs}^2 + \ldots\right). \quad \text{(A28)}$$

In Eq. (A28), M_0 is the mass of one atomic mass unit, and g_h is the value of the gravitational acceleration at the half-light level.

ACKNOWLEDGMENTS

Many people contributed to the success of this work. In particular, we thank the management staff, operations team, flight crew, and ground crew of the Kuiper Airborne Observatory for overcoming several serious, unanticipated problems and successfully getting the KAO into the occultation path. A reliable occultation prediction would not have been possible without the efforts of Otto Franz, Connard Dahn, Harry Guetter, Dick Walker, Jeff Pier, and Arnold Klemola. We appreciate an early alert from Doug Mink of the substantial shift of the predicted occultation track from its original location. Linda Cordella, Anita Killian, Steve McDonald, Alex Laats, Olga Kuhn, Joe Harrington, Richard Baron, and Tim Shephard helped prepare for the observations; Linda Cordella, Dara Norman, and Doug Williams assisted with the data reduction and analysis. We thank Jack Wisdom for loan of equipment and Dick French and Phil Nicholson for helpful discussions. We acknowledge David Tholen for communication of results prior to publication and thank Bill Hubbard for pointing out to us that the effects of limb curvature contribute a significant correction to the observed scale height. Comments from two anonymous referees are also appreciated. This work has been supported, in part, by NASA Grants NSG-7603, NSG-7526, NAG 2-475, and NSF Grant AST 8519518.

REFERENCES

Abramowitz, M., and I. A. Stegun 1972. *Handbook of Mathematical Functions with Formulas, Graphs, and Mathematical Tables*. U.S. Govt. Printing Office, Washington, DC.

Apt, J., N. P. Carleton, and C. D. Mackay 1983. Methane on Triton and Pluto: New CCD spectra. *Astron. J.* **270,** 342–350.

Aumann, H. H., and R. G. Walker 1987. IRAS observations of the Pluto–Charon system. *Astron. J.* **94,** 1088–1091.

Baum, W. A., and A. D. Code 1953. A photometric observation of the occultation of σ Arietis by Jupiter. *Astron. J.* **58,** 108–112.

Beletic, J. W., R. M. Goody, and D. W. Tholen. Orbital elements of Charon from speckle interferometry. *Icarus*, in press.

Bessell, M. S. 1976. *UBVRI* photometry with a Ga–As photomultiplier. *Publ. Astron. Soc. Pac.* **88,** 557–560.

Binzel, R. P., D. J. Tholen, E. F. Tedesco, B. J. Buratti, and R. M. Nelson 1985. The detection of eclipses in the Pluto–Charon system. *Science* **228,** 1193–1195.

Bosh, A. S., J. L. Elliot, S. E. Kruse, R. L. Baron, E. W. Dunham, and L. M. French 1986. Signal-to-noise ratios for possible stellar occultations by Pluto. *Icarus* **66,** 556–560.

Brosch, N., and H. Mendelson 1985. *Occultation by Pluto on 1985 August 19*. IAUC No. 4097.

Brown, G. N., Jr., and W. T. Ziegler 1980. Vapor pressure and heats of vaporization and sublimation of liquids and solids of interest in cryogenics below 1-atm pressure. *Adv. Cryog. Eng.* **25,** 662–670.

Buie, M. W., and U. Fink 1987. Methane absorption variations in the spectrum of Pluto. *Icarus* **70,** 483–498.

Buie, M. W., and D. J. Tholen 1986. The surface albedo distribution of the Pluto–Charon system. *Bull. Amer. Astron. Soc.* **18,** 821.

Chamberlain, J. W., and D. M. Hunten 1987. *Theory of Planetary Atmospheres: An Introduction to Their Physics and Chemistry*. Academic Press, New York.

Cruikshank, D. P. 1987. Pluto, Charon, and Triton: A review of their physical parameters, atmospheres, and surfaces. *Bull. Amer. Astron. Soc.* **19,** 858.

Cruikshank, D. P., C. B. Pilcher, and D. Morrison 1976. Pluto: Evidence for methane frost. *Science* **194,** 835–837.

Cruikshank, D. P., and P. M. Silvaggio 1979. Triton: A satellite with an atmosphere. *Astrophys. J.* **233,** 1016–1020.

Dunham, E. W., R. L. Baron, J. L. Elliot, J. V. Vallerga, J. P. Doty, and G. R. Ricker 1985. A high-speed, dual-CCD imaging photometer. *Publ. Astron. Soc. Pac.* **97,** 1196–1204.

Elliot, J. L., E. W. Dunham, R. L. Baron, A. W. Watts, S. P. Kruse, W. R. Rose, and C. M. Gillespie 1988. Image quality on the Kuiper Airborne Observatory. I. Results of the first flight series. In preparation.

Elliot, J. L., R. G. French, E. W. Dunham, P. J. Gierasch, J. Veverka, C. Church, and C. Sagan 1977. Occultation of ε Geminorum by Mars. II. The structure and extinction of the Martian upper atmosphere. *Astrophys. J.* **217,** 661–679.

Elliot, J. L., and J. Veverka 1976. Stellar occultation spikes as probes of atmospheric structure and composition. *Icarus* **27,** 359–386.

Fink, U., B. A. Smith, D. C. Benner, J. R. Johnson, H. J. Reitsema, and J. A. Westphal 1980. Detection of a CH_4 atmosphere on Pluto. *Icarus* **44,** 62–71.

Fox, J. J., and F. G. H. Tate 1930. Refractivity of all gases and vapors and of elementary substances in

higher signal-to-noise ratios and spectral resolution, which will improve our understanding of the structure, composition, and temporal behavior of this distant planet's atmosphere.

APPENDIX

The Slope of an Occultation Lightcurve Produced by a Small Planet

In this appendix we calculate the first and second order correction terms to the slope of the occultation lightcurve at the half-light level for an isothermal planetary atmosphere whose scale height is a significant fraction of the planetary radius. We base our calculation on the general methods and assumptions of previous derivations (Baum and Code 1953, Goldsmith 1963), but here we include the following additional effects: (i) the variation of gravity with planetary radius, so that the number density as a function of planetary radius, $n(r)$, is expressed by Eq. (1); and (ii) the partial focusing of the starlight by the curvature of the planetary limb perpendicular to the path of the starlight (Elliot *et al.* 1977).

The atmospheric occultation is illustrated in Fig. A1, where starlight is incident from the left. A ray having closest approach r to the center of a planet is refracted by an angle θ by its atmosphere and arrives at the observer at a distance ρ from the center of the planet's shadow (in a plane lying perpendicular to the path of the incident starlight). The shadow is at a distance D from the center of the planet. Since θ is a small angle, we can write the following geometrical relation:

$$\theta = \frac{\rho - r}{D}. \tag{A1}$$

Note that θ has a negative value in Fig. A1. We define the quantity ϕ_{cyl} as the stellar flux that would be received in the shadow for a cylindrical atmosphere (i.e., no limb curvature in the direction perpendicular to the incident starlight). The flux is normalized such that $\phi_{cyl} = 1.0$ for full stellar intensity and 0.0 when the starlight is completely extinguished. In the geometric optics approximation, the flux observed in the shadow will depend on the expansion, due to differential refraction, of a bundle of rays of radial width Δr at the planet to a radial width $\Delta\rho$ in the shadow. The expansion factor is $\Delta\rho/\Delta r$, so that ϕ_{cyl} is given by the reciprocal of this ratio:

$$\phi_{cyl} = \frac{dr}{d\rho}. \tag{A2}$$

The curvature of the planetary limb in the direction perpendicular to the incident starlight reduces the radius of the shadow relative to its level of closest approach in the planetary atmosphere. This effect enhances the starlight in the shadow by the ratio of the circumference of a circle of radius r at the planet to the circumference of radius ρ in the shadow. We denote the flux received in the shadow by ϕ_{ref}, and it is given by the equation

$$\phi_{ref} = \frac{r}{\rho}\,\phi_{cyl}(r) = \left(\frac{r}{\rho}\right)\frac{dr}{d\rho}. \tag{A3}$$

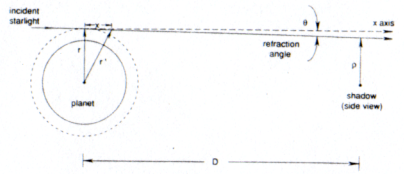

FIG. A1. Refraction by a planetary atmosphere. Starlight impinges on the atmosphere from the left and is refracted by an angle θ, due to the density gradient in the atmosphere. A ray that has closest approach r from the center of the planet travels a distance D and arrives at a radius ρ in the shadow. The x axis in the diagram lies along the original path of the incident ray. The path followed by the ray through the atmosphere is essentially along this path, since the extent of the atmosphere is negligible compared with the distance to the shadow. In this diagram, r' illustrates a radial coordinate within the atmosphere that is used as a variable of integration.

Being interested in the slope of the observed lightcurve, we need an equation for the derivative of ϕ_{ref} in the shadow, which can be found by differentiating the reciprocal of Eq. (A3) and making a further substitution for ϕ_{ref}:

$$\frac{d\phi_{ref}}{d\rho} = -\phi_{ref}^3\,\frac{\rho}{r}\left\{\left(\frac{\rho}{r}\right)\frac{d^2\rho}{dr^2} + \frac{1}{r}\left[\left(\frac{d\rho}{dr}\right)^2 - \frac{1}{\phi_{ref}}\right]\right\}. \tag{A4}$$

Using Eq. (A1), we can express the ratio and derivatives of ρ and r in terms of θ and its derivatives with respect to r:

$$\frac{\rho}{r} = 1 + D\,\frac{\theta}{r} \tag{A5}$$

$$\frac{d\rho}{dr} = 1 + D\,\frac{d\theta}{dr} \tag{A6}$$

$$\frac{d^2\rho}{dr^2} = D\,\frac{d^2\theta}{dr^2}. \tag{A7}$$

To proceed further we must establish the functional dependence of the refraction angle of the light ray, θ, on the distance of its closest approach to the center of the planet, r. We do this by finding the additional optical path (with respect to empty space), $\eta(r)$, traversed by a light ray making a closest approach r to the center of the planet. An equation for $\eta(r)$ is obtained by defining an x coordinate parallel to the incident starlight and integrating the refractivity of the atmosphere along its path through the atmosphere (see Fig. A1). We define a radial coordinate, r', whose origin is at the center of the planet; since θ is a small angle, x, r, and r' are related by

$$r'^2 = r^2 + x^2. \tag{A8}$$

Denoting Loschmidt's number by N_0 and the refractivity of the gas comprising the atmosphere (at standard temperature and pressure) as ν_{STP}, we can write the desired integral:

$$\eta(r) = \int_{-\infty}^{\infty} \nu_{STP}\,\frac{n(r')}{N_0}\,dx. \tag{A9}$$

We define r_h as the radius in the planetary atmosphere for which $\phi_{ref}(r) = \frac{1}{2}$, and at this radius the local scale height is H_h (see Eq. (2)). Evaluation of the integral in Eq. (A9) has been carried out to first order in $(1/\lambda) = rH_h/r_h^2$ by Chamberlain and Hunten (1987). In terms of our notation their result is

$$\eta(r) = \frac{\nu_{STP} n_h}{N_0}\sqrt{\frac{2\pi r^3 H_h}{r_h^2}}\left(1 + \frac{9rH_h}{8r_h^2} + \ldots\right)\exp\left[\frac{r_h^2}{H_h}\left(\frac{1}{r} - \frac{1}{r_h}\right)\right]. \tag{A10}$$

Note that a complete second order treatment should properly include another term in the series expansion appearing in Eq. (A10). We define $\delta = H_h/r_h$ and $u = r/r_h$. Written in terms of these dimensionless variables, Eq. (A10) becomes, to first order,

$$\eta(u) = \frac{\nu_{STP} n_h H_h^{1/2}\sqrt{2\pi r_h}}{N_0}\,u^{3/2}\left[1 + \frac{9}{8}(\delta u)\right]\exp\left[\frac{1}{\delta}\left(\frac{1}{u} - 1\right)\right]. \tag{A11}$$

The refraction angle undergone by a ray is given by the derivative of the additional optical path:

$$\theta = \frac{d\eta}{dr} = \frac{1}{r_h}\,\frac{d\eta}{du}. \tag{A12}$$

Evaluating this derivative, we find

$$\theta = -\frac{\nu_{STP} n_h\sqrt{2\pi r_h}}{N_0 H_h^{1/2}}\,u^{-1/2}\left[1 - \frac{3}{8}(\delta u) - \frac{45}{16}(\delta u)^2\right]\exp\left[\frac{1}{\delta}\left(\frac{1}{u} - 1\right)\right]. \tag{A13}$$

Obtaining Eq. (A13) through the differentiation of Eq. (A11) and other laborious algebraic manipulations occurring in the remainder of this appendix were carried out with the aid of the MACSYMA™ program (Symbolics 1985). Evaluation of the required first and second derivatives of θ yields

we use the two-stream approximation with a Lambert surface, we can express the observed geometric albedo, p_{obs}, in terms of the surface geometric albedo, p_s, and the vertical optical depth, τ_a,

$$p_{obs} = \frac{p_s}{\sqrt{2}} \exp[-2\sqrt{2}\,\tau_a]. \quad (22)$$

For the present geometric albedo (Tholen *et al.* 1987) of 0.61, as determined from the mutual events at phase 0.25, we find $\tau_a \leq 0.06$. This is well below our lower limit of 0.19 on the vertical optical depth, so, if the extinction is global, we can infer that the particles must predominantly scatter incident light rather than absorb it.

Another approach to limiting the surface radius is to extrapolate our atmospheric structure to smaller radii, until the pressure equals the surface atmospheric pressure. While possible in principle, this approach requires several assumptions, each of which needs careful examination: (i) Pluto's atmosphere is pure methane, (ii) its surface pressure is in equilibrium with solid methane, (iii) its surface temperature is known, and (iv) we can extrapolate our derived atmospheric structure to the surface. Pursuit of this approach is beyond the scope of this work, since it would involve development of a self-consistent model for Pluto that would include other data sets. In particular the IRAS data would have to be reexamined in terms of different surface radii.

We can, however, explore the consequences of our results with those of Sykes *et al.* (1987), who have related the IRAS fluxes at 60 and 100 μm to surface models for Pluto and Charon. Using the radii of Pluto and Charon found from the mutual events and certain assumptions about Pluto's surface albedo distribution, they infer a surface temperature of 58 ± 1°K, for which the equilibrium methane vapor pressure is 75 μbar (Brown and Ziegler 1980). If we assume that the temperature of Pluto's atmosphere changes to 58°K at the top of the extinction layer, we can extrapolate the pressure to smaller radii, as shown in the right panel of Fig. 4. This curve reaches a pressure of 75 μbar at a surface radius of 1013 km. For the pressure–altitude profile for this case shown in Fig. 4, we used Eq. (21) to calculate a methane column abundance of 12.6 mA. This is somewhat greater than the upper limit on the methane column abundance inferred from spectroscopic observations (Buie and Fink 1987), although the presence of the extinction might cause some revision in the interpretation of the spectra. A rigorous approach along these lines would require establishing the radius at which Pluto becomes optically thick to the IRAS photometric wavelengths, which might lie within the atmosphere rather than at the surface. If this "thermal radius" proves to be smaller than the radius adopted by Sykes *et al.* (1987), then the derived surface temperature will be greater than 58°K, implying a larger surface pressure for methane equilibrium models. These models of Pluto will be complicated by the uneven absorption of sunlight over Pluto's surface, due to its rotation and marked albedo variations, so that no single combination of temperature and vapor pressure would apply to the entire planet.

For a methane atmosphere, the minimum surface pressure that would be consistent with the occultation data is found by extrapolating the higher temperature curve through the extinction layer to the maximum surface radius permitted by the occultation data (see the left panel of Fig. 4). At this maximum surface radius, the pressure would be 3 μbar, which is the vapor pressure of methane at 50°K. This scenario would require an abrupt drop in temperature near the surface to be consistent with the thermal fluxes measured by IRAS. Again, the likelihood of thermal variations on Pluto due to its rotation and albedo variations implies a more complex situation.

A further complication introduced by the extinction is in the interpretation of Pluto's secular brightness changes. In particular, the secular dimming has been interpreted as evidence for polar caps (Buie and Tholen 1986, Marcialis 1988). While this may be the correct explanation, we should leave open the possibility that the secular albedo change is produced either by secular changes in the optical thickness of the extinction particles, perhaps as a function of insolation, or by evaporation of methane frost. According to Marcialis (1988), the minimum light—if due to polar caps—should have occurred in 1980. If the minimum is more closely tied to Pluto's perihelion in 1989, then one might look into alternative explanations for the secular dimming.

IX. CONCLUSIONS

Observations of the June 9, 1988, stellar occultation conclusively demonstrate that Pluto has an atmosphere. Our results are consistent with a methane atmosphere at 67 ± 6°K above about 1189 km from the center of Pluto, but they are also consistent with any other gas, or combination of gases, that have our measured ratio of temperature to mean molecular weight (4.2 ± 0.4°K/amu). In particular, a substantially nitrogen atmosphere at 117 ± 11°K would be consistent with the occultation results. The upper part of the atmosphere has a few nonisothermal features, as evidenced by spikes in both the immersion and emersion portions of the lightcurve.

Below the essentially clear region described above, there is an extinction layer that has an abrupt upper boundary and extends at least 46 km in depth. The detailed nature of this extinction layer is not known, but its existence seems inescapable if one is to explain the complete loss of starlight observed during the occultation. The alternative to the extinction explanation is to believe that the lower atmosphere has an extremely high mean molecular weight (~400). The boundary of the extinction layer may also be either a thermal boundary, below which the atmosphere is substantially cooler, or a composition boundary, below which the mean molecular weight is higher. Somewhere below the upper boundary of the extinction layer, the atmosphere must become cooler to be consistent with the IRAS thermal fluxes. The immersion and emersion lightcurves show identical structure of both the clear atmosphere and extinction layer to the limit of precision of our model fits.

The existence of an extinction layer that is optically thick at Pluto's limb means that the radius of Pluto's solid surface is uncertain. Consequently, we do not know the planet's density. We have presented a few approaches to constrain the value of the surface radius, but since this problem is so intricately connected with other observations of properties of Pluto, it should be possible to achieve tighter limits on possible values for the surface radius. We should emphasize that, although much of the interpretation of observations of Pluto has been based on the assumption of a pure methane atmosphere, we see no compelling evidence that this is the case, especially in the lower atmosphere. With the addition of the occultation data, the time appears opportune for determining the class of physical models that can meet the diverse collection of observational constraints on Pluto's atmosphere and surface properties.

The first results of the airborne data presented here can be improved and extended through further analysis. We expect to be able to improve the signal-to-noise of our airborne data (Stover and Allen 1987) and to analyze the observations with a more complete model and a more accurate geometrical solution. Numerical inversion may be attempted to see how the spikes affect the derived atmospheric structure, and we intend to explore more possibilities for the structure of the extinction layer. Also, combining the data from all observing sites will reveal whether the atmospheric structure varies with position on the planet. A more accurate value for the local gravity, which we can obtain from a geometrical solution that uses all the observations and an improved value for the mass of Pluto, will further enhance the analysis. Clearly it will be valuable to observe more stellar occultations by Pluto. Hopefully some will have

change in the lightcurve slope as being due to an impossible decrease in temperature (to ~3°K) or to an unlikely increase in the mean molecular weight of the atmosphere (to ~400). However, some combination of these effects may be occurring, so our interpretation of the parameters describing the extinction layer must be tempered with the understanding that extinction—while being the dominant effect—may be accompanied by a decrease in scale height.

We find an extinction scale height that is about half of that of the gas of the overlying atmosphere. Our observations also show that the extinction has great longitudinal extent around Pluto's limb. The KAO chord shown in Fig. 2 sampled starlight that passed through the atmosphere, perpendicular to the limb from both sides of the planet (Elliot *et al.* 1977). These zones correspond to the bold arcs in Fig. 2. Hence if the extinction were not present in any of the areas between our immersion and emersion points, and in the corresponding region on the opposite side of the planet, the lightcurve intensity would have risen above the level of Pluto alone. The small, broad bump on the left-hand side of the baseline (see Fig. 1) may be a manifestation of this effect.

Our data give no indication where the extinction particles are being formed. The logical possibilities for the location where these particles originate are (i) at the upper boundary of the layer, (ii) within the extinction layer itself, or (iii) at the surface of Pluto. We have explored the consequences of the first two possibilities by means of a simple continuity equation with a source term; more detail on this analysis will be presented in a subsequent publication. If the particles are being created in the clear atmosphere (for example, by photochemical reactions driven by solar UV radiation, followed by condensation at the top of the extinction layer) and are "raining out" to the surface, their velocity of descent would be inversely proportional to the number density of the gas. In this case the particles would be expected to acquire the scale height of the atmospheric gas. For methane, the extinction scale height (see Table IV) would imply a temperature of 40 ± 8°K in the extinction layer. Since a change in temperature at the boundary of the extinction layer is not included in the model, the change in lightcurve slope in this case would be caused by a combination of extinction and a lower value of the ratio $T/\bar{\mu}$ in the extinction layer. To investigate this situation requires an additional model parameter that would allow a scale height change in the gas at the onset of extinction. If the particles are being produced in the extinction layer itself at a rate proportional to the local gas density (reactions driven by cosmic rays being the likely physical mechanism), then the particle density would have a scale height one-half that of the gas. In this case our present model for the lightcurve would be correct. Finally, if the particles are produced at the surface and are raised to higher levels in the atmosphere by evaporating methane, for example, it is not at all clear what the vertical distribution would be, or why there would be an abrupt cap on the altitude of the particles.

Our understanding of the extinction in Pluto's atmosphere may be aided by comparison with other small, outer Solar System objects with atmospheres, namely Titan and Triton. Much has been learned about Titan from the Voyager encounters; the following information is from the review by Hunten *et al.* (1984). Titan's haze seems to be produced by a combination of reactions driven by solar UV radiation, magnetospheric charged particles, and cosmic rays. Its scale height is about 80% of that of the gas. For Pluto, we would not expect any magnetospheric charged particles, and the solar UV flux is lower by a factor of 10 than for that on Titan. However, the cosmic ray flux would be essentially the same. Thus, we would expect the scale height of Pluto's haze to be closer to half of the gas scale height than for the case of Titan. The top of Titan's haze occurs in its atmosphere where the number density is about 10^{15} and the temperature is about

170°K, higher in both cases than the conditions in Pluto's atmosphere. Although methane is present in Titan's atmosphere, its principal constituent is nitrogen, which might mean that the hazes in the two bodies have different origins. As mentioned previously, we cannot rule out the possibility that the principal constituent of Pluto's atmosphere is nitrogen also.

Evidence that Triton may have an atmosphere is circumstantial. The evidence consists of a spectrum showing features characteristic of methane (Cruikshank and Silvaggio 1979, Apt *et al.* 1983), its small phase coefficient (Goguen *et al.* 1988), and its lack of detectable photometric variability throughout the satellite's orbital period (Lark *et al.* 1988). This latter observation suggests that reflected light from Triton is not from the object's solid surface. Hence haze (or clouds) may be a common property of the atmospheres of Pluto, Titan, and Triton.

The existence of the extinction layer seriously complicates the determination of the surface radius of Pluto. Clearly the shape of the mutual event lightcurves will be affected by this layer, since the visible limb of Pluto will not be sharp. However, to first order, the radii measured by the mutual occultations and eclipses must refer to the visible disks of Pluto and Charon. At the level of accuracy of the analysis presented here, our unit optical depth level on the limb is consistent with the radius obtained by modeling the mutual events, but the solid surface could lie far below this level (see Fig. 4).

What is the surface radius of Pluto? We can place an upper limit on the surface radius as the radius that corresponds to the time when the star was last detectable. This is illustrated in the left panel of Fig. 4. With present information we see several approaches to placing lower limits on its value, and each of these involves extrapolating the observed atmospheric structure to lower altitudes, until a particular quantity exceeds a limit imposed by other observations of Pluto. Simply stated, these approaches are (i) the vertical optical depth of the extinction cannot be too great for purely scattering particles, or Pluto's rotational lightcurve would not have such a large amplitude; (ii) the vertical optical depth of the extinction cannot be too great for purely absorbing particles, or Pluto's albedo would not be so large; (iii) a methane atmosphere could not be too deep, or (a) the surface pressure would exceed the vapor pressure of methane, and (b) the amount of gaseous methane would exceed the limit on the column abundance of methane imposed by spectroscopic observations; and (iv) too small a surface radius would put the density of Pluto at impossibly large values. The last approach begs the question, however, since a primary use for the surface radius of Pluto is to establish its bulk density, which provides a first order constraint on acceptable interior models for the planet. The correspondence between density and surface radius is shown in the left panel of Fig. 4.

First we consider the lower limit on the surface radius imposed by extrapolating the extinction. In doing this we assume (i) the amplitude of Pluto's lightcurve is entirely due to surface albedo features on Pluto, with no contribution from Charon; (ii) that the observed extinction is global on Pluto, and we can extrapolate the exponential functional dependence of the extinction to the surface; and (iii) the extinction is purely scattering, with no absorption. Accepting these assumptions and considering an extreme model for the albedo variations on Pluto, we find that the vertical optical depth could not exceed ~0.5–1.0 before reducing the contrast below the observed value of ±0.15 mag (Marcialis 1988). Extrapolating the extinction to lower altitudes, we find the vertical optical depth reaches 1.0 at a radius of 1085 km, as shown in Fig. 4. We must recall, however, that Titan exhibits haze layers that are detached from its surface, which, if the case for Pluto, would invalidate this approach for establishing a lower limit to the surface radius.

If the extinction is purely absorbing and

1988). The uncertainty in M_{sys} given in Table III reflects the quoted error in the semimajor axis of the system. We calculated the mass of Pluto from the system mass by subtracting Charon's mass, using its radius obtained from the mutual events (see Table III), and assuming that it has a density of 2.0 ± 1.0 g cm^{-3}. The error bar in Pluto's mass reflects this uncertainty in Charon's density, as well as the error in M_{sys}. Finally, the value of g_h was calculated, and its error was estimated by quadratic addition of the errors in r_h and M_p. The ratio $T/\bar{\mu}$ obtained with Eq. (15) is 4.2 ± 0.4°K/amu.

These properties of Pluto's atmosphere are summarized in the left panel of Fig. 4. This is a diagram of the structure of Pluto's atmosphere, as derived from the occultation in terms of the model described in the previous section. The region probed—from the first detectable light loss until the star was last detectable—lies between 1462 and 1143 km from the center of Pluto. This zone lies between the dashed and solid circles in Fig. 2 and is also shown in Fig. 4. Relative values of radii within this scale are accurate within a few kilometers (within the context of the model, which postulates that the refractive part of the flux is continuous across the upper boundary of the extinction layer), but the placement of the scale has an estimated uncertainty of ±20 km. The sources of this uncertainty are (i) the errors in our preliminary geometrical solution and (ii) uncertainty in the position of the KAO. The top of the extinction layer lies 25 km below the half-light level. We observe a line-of-sight optical depth of 1.0 at 15 km below the top of the extinction layer, and we can no longer detect light from the star 46 km below the top of the extinction layer. This establishes a minimum thickness for the extinction layer; the corresponding lower limit on the vertical optical depth is 0.19. The scale height of the extinction layer derived from the model fits is about half that of the overlying atmosphere.

We can make further inferences about the structure of Pluto's atmosphere by assuming its composition. One likely atmospheric constituent is methane (Stern and Trafton 1984); certainly its spectral features are the only ones that have been identified in spectra of Pluto. One reason for assuming that methane is the major constituent is because it has the lowest molecular weight ($\mu = 16$) of the plausible constituents, which implies the lowest atmospheric temperature. If the atmosphere is composed entirely of methane, our model yields a temperature of 67 ± 6°K. For a greater mean molecular weight, the temperature would be greater in accordance with our measured value of $T/\bar{\mu}$. Under the assumption that the atmosphere is composed mainly of methane, we can calculate number density and pressure at the half-light level, using Eqs. (A27) and (A28) and the refractivity of methane at standard temperature and pressure (Fox and Tate 1930). These values have been tabulated in Table IV, along with other quantities of interest at the half-light level. The atmospheric structure under the pure methane assumption is shown in the right panel of Fig. 4. The solid line corresponds to our methane model temperature of 67°K. Below the onset of the extinction layer, we have plotted three dashed curves, since we cannot be sure of the temperature of the atmosphere. The lower curve is a continuation of the 67°K temperature, and the upper curve corresponds to a temperature of 40°K—the value for a pure methane atmosphere if we assume that the scale height of the extinction matches that of the gas. The middle curve corresponds to a temperature of 58°K, the result of the model of Sykes *et al.* (1987) from the IRAS data. Note that letting the scale height of the gas match that of the extinction in the extinction layer is inconsistent with the assumption used to fit the model of a constant scale height for the clear atmosphere. If the temperature does decrease in this region, then part of the drop in the lightcurve would be caused by the temperature drop. We shall pursue this type of model in later work.

TABLE IV

STRUCTURE OF PLUTO'S ATMOSPHERE

Region probed by the stellar occultation: $1143 \text{ km} < r < 1462 \text{ km}$	
Parameters derived from the lightcurve model	
Clear atmosphere, at the half-light level ($r_h = 1214 \pm 20$ km)	
Scale height (H_h)	59.7 ± 1.5 km
$T/\bar{\mu}$	4.2 ± 0.4°K/amu
Extinction layer	
Top ($r_{\tau 0}$)	1189 km[a]
Unit optical depth ($r_{\tau 1}$)	1174 km[a]
Thickness	≥46 km[a]
Vertical optical depth (τ_v)	≥0.19
Scale height	33.4 ± 6.9 km
Additional parameters based on CH_4 assumption	
For pure CH_4 ($\bar{\mu} = 16$), at the half-light level ($r_h = 1214 \pm 20$ km)	
$T = 67 \pm 6$°K	
$n_h = 8.3 \pm 10^{13}$ molecules cm^{-3}	
$p_h = 0.78$ μbar	
$\xi_h = 0.20 \pm 0.01$ m-am	

[a] Although the placement of the radius scale has an uncertainty of ±20 km, the relative radii of various levels should have uncertainties no greater than 1–2 km.

A quantity of interest for the pure methane model is the equivalent column abundance of methane, since this quantity can be inferred directly from spectroscopic observations. We denote Loschmidt's number by N_0 and the equivalent column abundance for the gas lying between a radius r and the top of the atmosphere by $\xi(r)$, which is found from the equation

$$\xi(r) = \int_r^{r_{max}} \frac{n(r')}{N_0}\, dr'. \qquad (19)$$

In order to relate this to the occultation results in the easiest way, we write the integral of Eq. (19) in two parts, one expressing the abundance of methane from an arbitrarily large radius down to our half-light radius, $\xi_h = \xi(r_h)$, and the other part expressing the methane abundance below the half-light radius. The reason for this approach is that, under the assumption of pure methane, ξ_h has a well-determined value from our data, while the extrapolation of $\xi(r)$ to lower altitudes becomes more model dependent. First we write an expression for ξ_h to first order in H_{obs}/r_h, using the correction term given by Chamberlain and Hunten (1987):

$$\xi_h = \frac{n_h H_h}{N_0}\left[1 + 2\frac{H_{obs}}{r_h}\right] = \frac{H_{obs}^{5/2}}{\nu_{STP} D\sqrt{2\pi r_h}}\left[1 + \frac{41}{8}\frac{H_{obs}}{r_h}\right]. \qquad (20)$$

Evaluating it, we find that $\xi_h = 0.20$ mA. Now we can rewrite Eq. (19) as

$$\xi(r) = \xi_h + \int_r^{r_h} \frac{n(r')}{N_0}\, dr'. \qquad (21)$$

Equation (21) can be used, with the numerical value of ξ_h, to establish the constraints imposed by the occultation data for atmospheric models containing only methane.

VIII. DISCUSSION

Our observations show a clear upper atmosphere that extends down to a radius of 1189 ± 20 km. If the atmosphere is isothermal and composed of pure methane, it has a temperature of 67 ± 6°K in this region, but we do not know its properties at altitudes greater than the outermost levels probed by this occultation—about 1462 km from the center of Pluto. According to our data, the clear atmosphere could be composed of any combination of gases whose mean molecular weight would yield a plausible temperature when combined with our measured ratio of 4.2 ± 0.4°K/amu. For example, if the atmosphere were composed entirely of nitrogen, the temperature derived from our data would be 117 ± 11°K.

Below the base of the clear atmosphere lies an extinction layer, and although we can place some constraints, it should be understood that we cannot uniquely specify the atmospheric structure in this region. In this paper we have interpreted our data in terms of a model that postulates (i) the basic isothermal structure of the atmospheric gas persists to lower altitudes, and (ii) extinction begins abruptly, with the "particles" causing the extinction being distributed according to their own scale height. The extinction model seems much more plausible than explaining the sudden

TABLE III

ADOPTED PARAMETER VALUES

Parameter	Symbol	Value	Reference
Mass of Pluto and Charon	M_{sys}	$(1.47 \pm 0.07) \times 10^{25}$ g	Beletic *et al.* (1988)
Mass of Pluto	M_p	$(1.29 \pm 0.11) \times 10^{25}$ g	
Radius of Pluto	R_p	1142 ± 21 km	Tholen and Buie (1988)
Radius of Charon	R_c	596 ± 20 km	Tholen and Buie (1988)
Gravity (at $r = r_h$)	g_h	58.3 ± 5.4 cm sec^{-2}	
Limb velocity for upper atmosphere	$v_\perp$	13.4 ± 0.2 km sec^{-1}	
Limb velocity for extinction layer	$v_\perp$	11.8 ± 0.2 km sec^{-1}	
Refractivity of methane[a]	ν_{STP}	4.38×10^{-4}	
Earth–Pluto distance	D	4.323×10^9 km	

[a] Mean value, integrated over the spectral response of our CCD chip.

model alone. The values of the fitted model parameters, along with their errors, are given in Table II. Except of course for the half-light times, the parameter values obtained for the immersion and emersion fits agree well within their formal errors from the model fits. Hence, our best estimate for the values of the model parameters would be the weighted average of the immersion and emersion values, and these averages are also given in Table II.

From the weighted means in Table II, we get a ratio of $s_p/s_* = 0.234 \pm 0.002$. This can be compared with the value of this ratio, 0.236 ± 0.001, found from averaging the photometry from 20 of the open-chip CCD frames taken prior to the occultation. This pre-occultation photometry was done by fitting a dual-image model to the images on these frames. The difference between the air mass for the pre-occultation frames and that during the occultation observations was only 0.008 of a standard air mass at sea level, so color effects should be negligible, even though we used no filter for either set of data. Hence we conclude that the star was totally occulted, within the small uncertainty of our photometric measurements.

VII. STRUCTURE OF PLUTO'S ATMOSPHERE

We can use the results of our model fits in Table II and other information to establish the structure of Pluto's atmosphere, as learned from the stellar occultation. The first step in this process is to convert the model quantities h_{obs}, h_τ, χ_0, and χ_1 to spatial dimensions in Pluto's atmosphere. To do this conversion, we need the limb velocities. Mean values appropriate for the upper atmosphere and the extinction layer are given in Table III, where their errors reflect present uncertainties in the occultation geometry. Although a thermal gradient in the upper atmosphere would produce a lightcurve having the same shape as that for an isothermal atmosphere (Goldsmith 1963), for now we shall make the simpler assumption that the atmosphere is isothermal in this region. We find $H_{obs} = 59.2 \pm 1.5$ km, and using this we have calculated values for $r_{\tau 0}$ and $r_{\tau 1}$, which are given in Table IV. Also, we have used Eq. (6) to convert the observed scale height from the lightcurve to the scale height in the atmosphere, H_h.

Another quantity of interest is the ratio of temperature to mean molecular weight in this region:

$$\frac{T}{\bar{\mu}} = \frac{g_h H_h}{R_0}. \qquad (18)$$

Evaluation of this ratio requires a value for the local gravity, g_h. In computing g_h we used the combined mass of Pluto and Charon, M_{sys}, appropriate for a semimajor axis of 19,640 ± 320 km (Beletic *et al.*

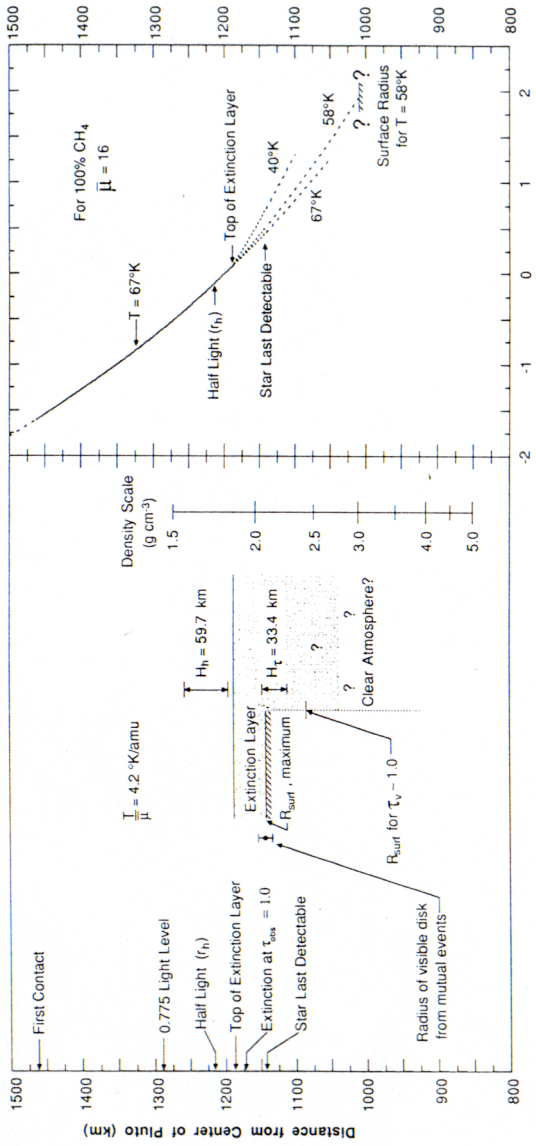

FIG. 4. Vertical structure of Pluto's atmosphere. This figure summarizes results from least-squares model fits to the occultation lightcurve. The left panel shows the most direct information from the occultation data, while information in the right panel is based on the assumption of a pure methane atmosphere. The distance from the center of Pluto at which the signal first begins to drop occurs at approximately 1462 km. At 1189 km, there is an abrupt change in the slope of the lightcurve, indicating the presence of an extinction layer. These features can be fit using a model that consists of an isothermal atmosphere and an extinction layer that has an abrupt upper boundary. From the model we find the scale height of the isothermal atmosphere and the scale height of the extinction. The occultation last probes the atmosphere at a height of 1143 km. This height may be the surface of Pluto, meaning that the extinction layer extends down to the surface, or the surface may still be several hundreds of kilometers below this point, with clear atmosphere in between. From the measured scale height, we find the ratio of temperature to mean molecular weight, $T/\bar{\mu}$. A likely major constituent would be methane; for pure methane, the temperature would be 67 ± 6°K. A pressure–altitude curve for this case is shown in the right-hand panel. Below the extinction layer, we have plotted three possibilities for the temperature: (i) a continuation of the 67°K curve from the upper atmosphere; (ii) an abrupt change to 40°K, the temperature for methane corresponding to the extinction scale height; and (iii) 58°K, which corresponds to one interpretation of the IRAS data. If this latter case is correct, Pluto's surface radius would be just over 1000 km, and the planet would have a density of about 3.0 g cm^{-3}.

We also define two particular values for χ: χ_0, which corresponds to the radius at the top of the extinction layer, $r_{\tau 0}$ (above which there is no extinction), and χ_1, which corresponds to the radius, $r_{\tau 1}$, at which the line-of-sight optical depth is unity in the extinction layer:

$$\chi_0 = \frac{r_{\tau 0} - r_h}{H_{obs}} \tag{13}$$

$$\chi_1 = \frac{r_{\tau 1} - r_h}{H_{obs}}. \tag{14}$$

In our model, the extinction has a scale height H_τ, and we define the parameter h_τ as the ratio of this scale height to the apparent velocity perpendicular to the limb: $h_\tau = H_\tau / v_\perp$. Neglecting a factor of $(\chi/\chi_1)^{1/2}$, we can now write the equation for $\tau_{obs}(r)$:

$$\tau_{obs}(r) = \frac{\operatorname{erf}\left[\sqrt{h_{obs}(\chi_0 - \chi)/h_\tau}\right] \exp[h_{obs}(\chi_1 - \chi)/h_\tau]}{\operatorname{erf}\left[\sqrt{h_{obs}(\chi_0 - \chi_1)/h_\tau}\right]}. \tag{15}$$

The observed stellar flux $\phi(t)$, which is normalized analogously to $\phi_{ref}(t)$, is related to $\phi_{ref}(t)$ and the observed optical depth, $\tau_{obs}(r)$, by the equation

$$\phi(t) = \phi_{ref}(t) \exp[-\tau_{obs}(r)]. \tag{16}$$

Finally, we can express the occultation signal versus time, $s(t)$, in terms of the stellar flux $\phi(t)$, the signal from Pluto s_p, and the signal from the unocculted star, s_*:

$$s(t) = s_p + s_* \phi(t). \tag{17}$$

The seven model parameters that can be determined from the data are summarized in the first column of Table II. Starting with initial values for the seven model parameters, the prescription for calculating $s(t)$ in terms of the model parameters is first to use Eq. (7) to find $\phi_{ref}(t)$, from which one then calculates $\tau_{obs}(r)$ with Eqs. (12)–(15) and then completes the process with Eqs. (16) and (17). Note that nowhere in this procedure does one have to use a value for $v_\perp$, so that the model fits are independent of its value—except for the assumption that it does not change appreciably during those portions of the immersion and emersion lightcurves where there is sufficient stellar signal to produce a significant effect on the model fits.

TABLE II

RESULTS OF MODEL FITS

Model parameter	Units	Immersion	Emersion	Weighted mean
Signal levels				
Pluto (s_p)	ADU[a]	127.6 ± 1.7	125.9 ± 1.7	126.8 ± 1.2
Star (s_*)	ADU[a]	541.9 ± 2.3	542.7 ± 2.3	542.3 ± 1.6
Isothermal atmosphere				
Time of half-light (t_h)	UTC	10:36:43.79 ± 0.19	10:38:09.75 ± 0.20	
"Scale height" (h_{obs})	sec	4.341 ± 0.148	4.468 ± 0.119	4.418 ± 0.093
Extinction layer				
"Scale height" (h_τ)	sec	3.049 ± 1.035	2.729 ± 0.711	2.832 ± 0.586
Top ($\chi_{\tau 0}$)	[b]	−0.442 ± 0.031	−0.394 ± 0.031	−0.418 ± 0.022
Unit optical depth ($\chi_{\tau 1}$) (at limb)	[b]	−0.676 ± 0.037	−0.679 ± 0.038	−0.677 ± 0.027

[a] Analog-to-digital units (ADU) give signal per 0.2 sec integration time. There are approximately 14 electrons per ADU. See Dunham *et al.* (1985) for description.

[b] These quantities are dimensionless.

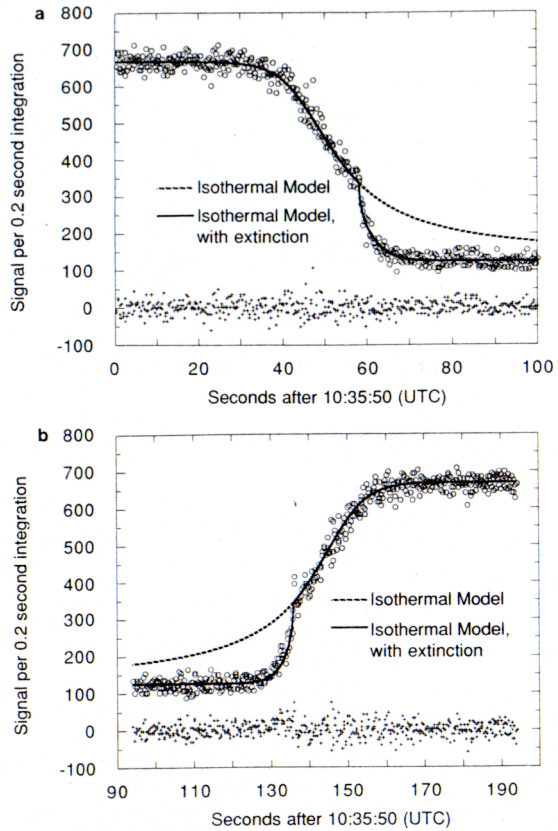

FIG. 3. Data, model, and residuals: (a) immersion, (b) emersion. Time is plotted along the horizontal axis, and signal level is plotted along the vertical axis. Data are represented by open circles. The dashed line is the curve representing an isothermal atmosphere model with a scale height of 59.7 km. The solid line represents an isothermal atmosphere with an extinction layer that abruptly begins at 1189 (±20) km from the center of Pluto. The vertical optical depth of the extinction is ≥0.19. The residuals (data − model) from the model fit are plotted as crosses.

VI. MODEL FITS TO THE DATA

The model described in the previous section was fitted by least squares to data intervals of 100 sec, for both the immersion and emersion portions of the lightcurve. The two intervals chosen had an overlap of 6 sec within the portion of the lightcurve showing a total occultation. The model fits are shown, along with the data and residuals, in Figs. 3a and 3b, where the exact interval of data fitted by the model has been plotted. In each figure, the isothermal model that matches the upper part of the lightcurve has been extended with a dashed line, in order to illustrate that the isothermal model with extinction provides a much better fit to the data than the isothermal

height change to be an unacceptable explanation, since it would imply a highly unlikely physical state for Pluto's atmosphere.

Finally, as we considered extinction to be the cause for the change in slope of the lightcurve, we experimented with several ways of introducing extinction into the model. Absorbing material that was uniformly mixed with the clear atmosphere could produce a lightcurve that dropped faster than a curve for an isothermal atmosphere, but this type of model could not produce the abrupt change of slope seen in our data. The type of extinction model that best matches the data postulates a clear upper atmosphere, overlying an extinction layer. The extent of the extinction layer is sufficient to extinguish completely the light from the star in our data. In this model we shall assume that the gas is everywhere isothermal and assume that the extinction has an exponential distribution at altitudes below the level where it begins. The distribution of the isothermal gas is unaffected by the extinction layer, and we use an abrupt transition from zero extinction above the layer to the magnitude of the extinction at the upper boundary of the layer.

We obtain an equation for the model lightcurve by (i) finding the equation for the lightcurve produced by an occultation by an isothermal atmosphere in which the variation of gravity is significant within a scale height and then (ii) adding the effect of an extinction layer. First we write an equation that describes the number density, $n(r)$, as a function of the radius r from the center of Pluto. Defining R_0 as the gas constant, G as the gravitational constant, $\bar{\mu}$ as the mean molecular weight of the gas, M_p as the mass of Pluto, r_h as a photometric reference radius (for which we use the half-light radius), and $n_h = n(r_h)$, we can write (Chamberlain and Hunten 1987)

$$n(r) = n_h \exp\left[\frac{GM_p\bar{\mu}}{R_0T}\left(\frac{1}{r} - \frac{1}{r_h}\right)\right]. \quad (1)$$

It will prove convenient to define the local scale height as the parameter, $H(r)$, where

$$H(r) = \frac{R_0T}{\bar{\mu}g(r)}, \quad (2)$$

where $g(r)$ is the local gravity, which is given by the equation

$$g(r) = \frac{GM_p}{r^2}. \quad (3)$$

Now we can rewrite Eq. (1) in terms of $H_h = H(r_h)$:

$$n(r) = n_h \exp\left[\frac{r_h}{H_h}\left(\frac{r_h}{r} - 1\right)\right]. \quad (4)$$

For a clear atmosphere, a distant observer will see the starlight dim by the process of differential refraction. We define $\phi_{ref}(t)$ as the stellar intensity (produced by this process only), observed as a function of time, normalized such that $\phi_{ref}(t) = 1.0$ for full stellar intensity and $\phi_{ref}(t) = 0.0$ for a total occultation of the star. Goldsmith (1963) has shown that the functional form of $\phi_{ref}(t)$ for an atmosphere with a scale height gradient closely matches that of an atmosphere with no gradient. To obtain the true scale height of the atmosphere for this case, one must distinguish between the true scale height of the atmosphere (at the half-light level), H_h, and the scale height that would be derived from the lightcurve, the "observed scale height" or H_{obs}, by fitting a model under the assumption of no scale height gradient. In fact, the correction term derived by Goldsmith is just the difference in slope of the lightcurve at the half-light level that is caused by the scale height gradient.

In the Appendix we have extended this approach to obtain the change in the lightcurve slope due to the effects of the curvature of the planetary limb (to second order in H_{obs}/r_h), as well as to the scale height gradient caused by the $1/r^2$ gradient in the gravitational potential. We find that the observed scale height, H_{obs} (as defined by the lightcurve slope), is related to the true atmospheric scale height by

$$H_{obs} = H_h\left[1 - \frac{1}{2}\frac{H_h}{r_h} + \frac{59}{8}\left(\frac{H_h}{r_h}\right)^2\right]. \quad (5)$$

Written in terms of a solution for H_h, Eq. (5) becomes

$$H_h = H_{obs}\left[1 + \frac{1}{2}\frac{H_{obs}}{r_h} - \frac{55}{8}\left(\frac{H_{obs}}{r_h}\right)^2\right]. \quad (6)$$

By denoting that component of the apparent velocity of the star that is normal to the limb of Pluto as $v_\perp$ and defining $h_{obs} = H_{obs}/v_\perp$, we can write an equation that relates the normalized stellar flux to the observation time, t, and these parameters (Goldsmith 1963):

$$\frac{t - t_h}{h_{obs}} = \left(\frac{1}{\phi_{ref}(t)} - 2\right) + \ln\left(\frac{1}{\phi_{ref}(t)} - 1\right). \quad (7)$$

In Eq. (7), t_h is the (half-light) time when the stellar intensity has been reduced to exactly 0.5 of its unocculted value—due to differential refraction alone, and we let this define r_h, the photometric reference level (half-light radius) in Pluto's atmosphere. Equation (7) does not include the added intensity coming from the limb on the opposite side of the planet (Elliot *et al.* 1977). Omission of this effect is a reasonable approximation to make, since the extinction reduces the lightcurve to the level corresponding to the signal from Pluto alone before light from the opposite limb would affect the lightcurve. Another assumption used in deriving Eq. (7) is that $v_\perp$ is constant. Although this is not strictly true, its value deviates only ± 0.7 km sec^{-1} from its value of 13.4 km sec^{-1} at the midtime of the 18-sec time interval that encompasses the main change in signal due to refraction.

In addition to the dimming of starlight due to differential refraction, light is also lost by extinction. We model this by assuming a volume scattering and absorption coefficient, $\kappa(r)$, that follows an exponential distribution with scale height, H_τ, below a radius, $r_{\tau 0}$. At radius $r_{\tau 1}$, where the observed line-of-sight optical depth has a value 1.0, the absorption coefficient has the value κ_1:

$$\kappa(r) = \begin{cases} 0, & r > r_{\tau 0} \\ \kappa_1 \exp[-(r - r_{\tau 1})/H_\tau], & r \le r_{\tau 0}. \end{cases} \quad (8)$$

With the aid of Eq. (8) we can write an equation for the optical depth encountered for radiation impinging on the atmosphere from an external source and penetrating to a depth r. We shall refer to this as the vertical optical depth, $\tau_v(r)$. For $r > r_{\tau 0}$ the vertical optical depth is zero, but for $r < r_{\tau 0}$ we have

$$\tau_v(r) = \int_r^{r_{\tau 0}} \kappa(r')dr' = \kappa_1 H_\tau \exp\left[\frac{r_{\tau 1}}{H_\tau}\right]\left\{\exp\left[-\frac{r}{H_\tau}\right] - \exp\left[-\frac{r_{\tau 0}}{H_\tau}\right]\right\}. \quad (9)$$

The optical depth observed along the line of sight during the occultation, $\tau_{obs}(r)$, can be calculated explicitly, by making the approximation $r_h \gg H_\tau$, and using the usual approximations for integration along the line of sight (Baum and Code 1953, Goldsmith 1963). We define an x coordinate as being along the line of sight, with closest approach r to the planet. The upper limit of integration is $x_{max} = [2r_h(r_{\tau 0} - r)]^{1/2}$:

$$\tau_{obs}(r) = 2\kappa_1 \exp\left[\frac{-(r - r_{\tau 1})}{H_\tau}\right] \int_0^{x_{max}} \exp\left[\frac{-x^2}{2r_hH_\tau}\right] dx. \quad (10)$$

The optical depth observed along the line of sight is given by the equation

$$\tau_{obs}(r) = \kappa_1\sqrt{2\pi r_hH_\tau}\exp\left[\frac{(r_{\tau 1} - r)}{H_\tau}\right] \mathrm{erf}\left[\sqrt{\frac{(r_{\tau 0} - r)}{H_\tau}}\right], \quad (11)$$

where *erf* refers to the error function (Abramowitz and Stegun 1972).

Calculation of $\tau_{obs}(r)$ is most conveniently carried out in terms of more fundamental parameters describing the atmosphere by defining the dimensionless parameter, $\chi(r)$:

$$\chi(r) = \frac{r - r_h}{H_{obs}} = \ln\left(\frac{\phi_{ref}(t)}{1 - \phi_{ref}(t)}\right). \quad (12)$$

TABLE I

STATION LOCATIONS AND OCCULTATION TIMES

Station	Event[a]	Longitude (east)	Latitude	Altitude (km)	Time for 0.775 light (UTC)	Radial residual (km)
Charters Towers	I	146°18′26″.3	−20°00′31″.3	0.285	10:40:43.7	−16
	E				10:42:10.8	−12
Hobart	I	147°25′52″.5	−42°50′57″.3	0.310	10:40:32.5	15
	E				10:41:27.5	−16
KAO[b]	I	−170°40′12″	−20°25′06″	12.5	10:36:35.1	8
	E	−170°29′48″	−20°14′48″	12.5	10:38:18.8	21

[a] I for immersion and E for emersion.

[b] Positions of KAO at the event times are the raw data from the Omega navigation system, which have a systematic error ≈10–15 km.

sponds to half of the drop reported from Tasmania. Isothermal fits to the portions of the data shown in Fig. 1 above the sharp drops gave the 0.775 light times given in Table I for the KAO. The KAO coordinates, also given in Table I, have a systematic error of about 15 km, which was the error recorded by the inertial navigation system upon landing in American Samoa. Unfortunately, only the magnitude of the error and not its direction was recorded. The coordinates of the other sites and their times of 0.775 light are also given in the table. A least-squares fit of a circle to the six occultation times from the three data sets previously discussed was carried out by minimizing the sum of the squared radial residuals. This solution yields a radius at the 0.775 light level of 1271 ± 9 km. This radius is that of Pluto's shadow crossing the Earth and must be corrected for refraction effects by Pluto's atmosphere in order to find the corresponding distance from the center of Pluto. All radial distances that we subsequently discuss have had the refraction correction incorporated, so that they refer to radial distances at Pluto—not in its shadow.

The residuals of the KAO immersion and emersion points from this circular solution were 8 and 21 km outside (at a greater radius than) the circular solution. Considering that the uncertainty in the KAO position would be greater than the ground stations, we can reduce the residuals of the KAO chord considerably by assuming that the KAO chord was actually south of the positions given in Table I by about 15 km. In our later analysis we have used velocities that correspond to this shift, and we note that the difference in the limb velocity corresponding to this shift (in the region of interest) is 0.2 km sec^{-1}. The resulting chord as seen from the KAO is shown in Fig. 2, where we have also shown the chords corresponding to the other observations used in our preliminary geometrical solution. The dashed circle corresponds to the level in the atmosphere at which we could first detect a dimming of the star, while the solid circle corresponds to the radius at which the star was last detectable in our data.

V. MODEL LIGHTCURVE

Our approach for using the lightcurve of Fig. 1 to learn the structure of Pluto's atmosphere is to fit a model lightcurve to these data; the first step in this procedure is to identify the appropriate model. Some preliminary trials showed that an isothermal model would match the top of the curve, but it could not follow the steepening slope in the lightcurve that occurs when the stellar intensity falls below about 0.4 of its unocculted value. Three explanations for the slope increase were considered: (i) occultation by the limb of Pluto's solid surface; (ii) an abrupt change in the atmospheric scale height of a clear atmosphere to a smaller value at lower altitudes; and (iii) extinction in Pluto's atmosphere. If the change in slope were caused by encountering the limb of Pluto's solid surface, the scale of the toe of the curve would be set by a combination of the following effects: (i) diffraction by the limb, (ii) the angular diameter of the occulted star, and (iii) possible turbulent scattering by Pluto's atmosphere near the surface. The distance in the shadow between the point where the change in slope occurs and where the intensity reaches zero is about 80–100 km—10 times greater than could be accounted for by diffraction (French and Gierasch 1976). Furthermore, the toe of the curve cannot be accounted for by convolution of a sharp drop with the intensity profile of the occulted star, since, on the basis of its colors (Bosh *et al.* 1986), its angular diameter would be expected to project only about 0.8 km at the Earth–Pluto distance. Also, scattering by possible turbulence in Pluto's atmosphere would not be nearly large enough to explain the toe of the curve, since the lightcurve does not show evidence of strong scintillations (Hubbard *et al.* 1978).

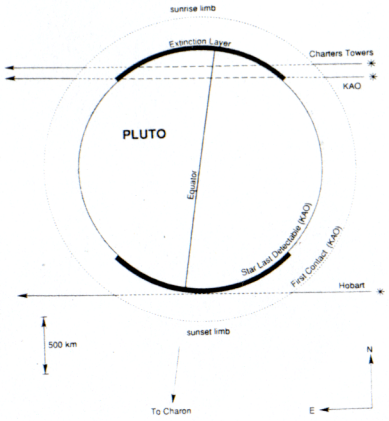

FIG. 2. Apparent paths of the occulted star relative to Pluto. The tracks shown refer to the three observing sites whose timings were used in our preliminary geometrical solution: the Lowell expedition to Charters Towers, in northeastern Australia; the Kuiper Airborne Observatory (KAO); and the University of Tasmania Observatory in Hobart, Tasmania. The coordinates of these sites are given in Table I. For the KAO, the position angle of the star's apparent track is 88°.76, and the apparent velocity of the star relative to Pluto is 18.45 km sec^{-1}. The outer dashed circle indicates the radius at which we could first detect the star being occulted, and the solid circle corresponds to the radius at which we could last detect light from the star. The bold arcs represent regions where Pluto's atmosphere has an extinction layer, as probed by the KAO data, and the stippled arcs show where the extinction layer would be if it surrounds the planet. Note that the indicated levels in Pluto's atmosphere correspond to their radii on Pluto, and not to their refracted radii in the shadow. The relative positions of the occultation chords, however, correspond to their relative positions in the shadow. If one plotted these chords as a function of the position probed in Pluto's atmosphere, they would exhibit substantial curvature, due to refraction (see Fig. A1).

The second explanation for the steepening slope—an abrupt change in scale height—cannot provide an adequate model for the lightcurve either. The main problem with such a model is that the observed minimum intensity cannot be achieved. The minimum lightcurve intensity (normalized to the unocculted intensity of the star) for a purely refractive occultation by a planet with an atmospheric scale height, H_h, and half-light radius, r_h, is about $16H_h/3r_h$ (Elliot *et al.* 1977). As we shall see later, using values for these parameters appropriate for the upper part of the lightcurve, we would predict a minimum value of 0.26 for the normalized intensity of the lightcurve, while our data show the actual value to be −0.002 ± 0.003. For the purposes of discussion, we place 0.01 as an upper limit (4σ) on the amount of residual stellar flux at the base of the lightcurve. Hence, adopting a purely refractive model would lead to unrealistically small values of the scale height for the lower part of the curve, which would imply an abrupt transition to some combination of an unphysically low temperature (~3°K) and a gas of very high molecular weight (~400). Therefore, we consider the scale

on Pluto's barycentric motion. Photometric observations of this occultation have been reported from eight sites (See *IAU Circs.* Nos. 4611, 4612, and 4620; Hubbard *et al.* 1988).

In this paper we present observations of the stellar occultation by Pluto, recorded with a high-speed CCD photometer attached to the 0.9-m telescope aboard the Kuiper Airborne Observatory (KAO). We develop a model for the occultation lightcurve that includes extinction, and, from the model fits to the lightcurves, we derive the structure of Pluto's atmosphere in the regions probed by the occultation. Also, we explore the possible physical states of the atmosphere on the assumption that it is composed entirely of methane, and we discuss the implications of our results as they relate to the interpretation of other observations of Pluto.

II. OBSERVATIONS

The direct CCD chip on the SNAPSHOT photometer (Dunham *et al.* 1985) was set up with an optical reduction factor of 3.3, which, in combination with the 0.9-m telescope on the KAO, produced a scale of 1.1 arcsec/pixel. In order to achieve a high signal-to-noise ratio by detecting the maximum amount of light from the occulted star, no filter was used for observations of the occultation. Hence, the wavelength response was that of the CCD chip itself (Dunham *et al.* 1985). The airborne seeing at the time of the event produced an image diameter of about 4 arcsec for 50% enclosed light. Since the images of Pluto and Charon were separated by less than an arcsecond, all photometry of Pluto includes the light from Charon as well. To avoid unnecessary repetition, references to the light from "Pluto" should be understood to mean the combined light from Pluto and Charon, unless specifically stated otherwise.

The flight plan of the KAO was devised to put the aircraft on the center line of the occultation ground track at the event's predicted midtime of 10:37:30 UT. However, an unavoidable delay in takeoff from Hickam AFB in Honolulu and head winds en route prevented the KAO from going as far south as originally planned, and observations were carried out about 120 km north of the predicted center line. Our data system clock was synchronized with WWVH just before takeoff. Three hours prior to the occultation observations, a series of 44 frames (480 rows, 390 columns), each having an exposure of 30 sec, were taken of the field containing Pluto and the star to be occulted. Twenty-two of these were exposed with no filter and the other twenty-two with an *R* filter (Bessell 1976). The images of Pluto and the star were separated by 12 arcsec. For the occultation itself, a 50 × 50-pixel frame containing Pluto and the star was recorded every 0.2 sec. Data recording began at 10:27:30 UTC and lasted for 20 min, which produced a total of 6000 images. Following the occultation data series, 16 full-size frames with no filter were exposed before observations were concluded. On these the images of Pluto and the star were blended.

III. OCCULTATION LIGHTCURVE

Since the CCD chip has been shown to have uniform response over the region containing the star and Pluto, correction for flat field was not necessary. A lightcurve was produced from the raw images by first finding the center of each image within the 50 × 50 frame by the technique of "marginal analysis" (Elliot *et al.* 1988). Then the signals from all pixels within a synthetic aperture were summed, and the background (as determined from an annulus surrounding the synthetic aperture) was subtracted. The synthetic aperture had a radius of 5 pixels (the corresponding aperture diameter was 11 arcsec), and the annulus used for establishing the background had an inner radius of 5 pixels and an outer radius of 15 pixels.

The section of the resulting lightcurve surrounding the occultation is shown in Fig. 1. Note that the curve appears symmetric, with a flat bottom. The bottom level corresponds to the signal from Pluto within the measurement error of 1% of the signal from Pluto (0.2% of the signal from the star), as determined from the frames of Pluto and the star taken prior to the occultation. Hence, within this uncertainty, the star was totally occulted. The shoulders of the curve near full intensity are characteristic of an occultation by an isothermal atmosphere, in which the main process causing the starlight to dim is differential refraction (Baum and Code 1953). However, slightly below half intensity the curve becomes much steeper than would be expected from an isothermal atmosphere, and the flat bottom of the curve is not consistent with a lightcurve produced by an isothermal atmosphere: another process must be operating. A few sharp spikes are present in both the immersion and emersion sections of the curve. Such features have been more frequent and pronounced in stellar occultation data obtained for other planets. The existence of such features in the present data indicate temperature variations of a few percent in Pluto's atmosphere, on scales of a few kilometers or less (Elliot and Veverka 1976).

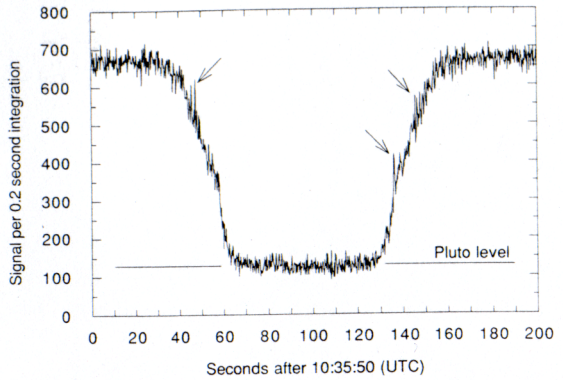

FIG. 1. Lightcurve of the stellar occultation by Pluto. Time is plotted along the horizontal axis, and signal level is plotted along the vertical axis. The signal is derived from circular aperture photometry, and is given as total signal per 0.2 sec integration. The signal-to-noise ratio for these data, defined as the ratio of the unocculted stellar signal to the rms noise, is approximately 33 : 1 for each integration. The gradual decline evident on immersion is indicative of an isothermal atmosphere. Near the half-light point, the slope of the lightcurve increases and then falls to the level of Pluto alone (shown by the solid line as determined from photometry several hours prior to the occultation), indicating a total occultation of the star. The curve is symmetric about the midpoint which occurs at 10:37:27 UTC. The lightcurve spikes are identified by the arrows.

IV. GEOMETRY OF THE OCCULTATION

Before we can learn the structure of Pluto's atmosphere from the lightcurve of Fig. 1, we need to establish the relationship of our occultation chord to the center of Pluto. To accomplish this, we have generated an approximate solution for the occultation geometry from three data sets: the KAO data described in this paper; the occultation data obtained by the Lowell Observatory expedition to Charters Towers, in northeastern Australia; and published timings for the chord obtained from Hobart, Tasmania (Watson *et al.* 1988). Since the Tasmanian lightcurve did not fall to the usual reference level of half-intensity, we have defined the level for our geometrical reference radius to be that of the 0.775 light level, which corre-